Proceedings of International Conference on Technology and Social Science 2017
Invited Paper

Damped Acoustic Analysis of a Car Cabin with Several Porous Materials

Yoshio Kurosawa[1, a], Takao Yamaguchi[2, b]

[1]Teikyo university, 1-1 Toyosatodai, Utsunomiya, Tochigi 320-8551, Japan

[2]Gunma university, 1-5-1 Tenjin-cho, Kiryu, Gunma 376-8515, Japan

[a]<ykurosawa@mps.teikyo-u.ac.jp>, [b]<yamagme3@gunma-u.ac.jp>

Keywords: Porous material, Car, FEM, Noise, Damping

Abstract. We created a test piece that simulates the upper back of a car. We measured the change in sound insulation from the sound-source side to the cabin side with breathable trim (urethane foam or felt). We created a finite-element model to calculate the acoustic-damping properties. Using urethane foam and felt to model the complex effective density and bulk modulus of the internal air, we sought the loss factor from the decay contribution of each sound-absorbing element employed in modal damping of the space. An experiment was conducted to verify this analysis, and it was found to be of sufficient accuracy, meaning that the sound-absorbing-material-thickness-dependent damping in an actual car could be accurately calculated by this technique.

1. Introduction

Recently, it has been thought important to design cars with comfortable interiors, and this goal can be facilitated by using lightweight soundproof materials to dampen noise. Although interior materials, such as the trim on the upper back and doors, have conventionally been made of resins such as impermeable polypropylene, more permeable materials such as hard felt, urethane foam, and the like are beginning to be employed more widely. Although these materials have been evaluated in terms of weight (i.e., whether they are lightweight compared with resin), intensity, and rigidity, their sound absorption and insulation properties are not fully understood. Conventional research employs the sound-property-prediction technique (the transfer-matrix method [1,2]), which assumes an infinite plate. However, the complicated nature of this calculation results inadequate accuracy.

In this study, the complex density and bulk modulus of urethane foam and felt were identified from the propagation constant and characteristic impedance obtained by the improved two-cavity method [3] using the impedance tub. The permeable trim is judged in the car's cabin, which is divided from the trunk by a porous object. A test piece imitating the upper back of a car is created, its acoustic properties are analyzed by measurement and the finite-element method.

2. Analytical Method

2.1 Discrete Equation for Sonic Fields Contained in Sound-Absorbing Materials

We discretize sonic fields contained in sound-absorbing materials using a finite-element method. In this study, the Helmholtz equation, which is suitable for a homogeneous sound field, is not used, because gas and the sound-absorbing materials are mixed in a complicated manner. Thus, we adopt the following approach. Under the assumption of infinitesimal amplitude, the equations of motion of an inviscid compressive perfect fluid undergoing periodic oscillation can be expressed as follows: [4,5]

$$-\text{grad}\ p = -\rho\omega^2\{U\} \tag{1}$$

The continuity equation is written as

$$p = -E \operatorname{div}\{U\} \tag{2}$$

where p is the sound pressure, $\{U\}$ is the particle-displacement vector, ω is the angular frequency, and E and ρ are the bulk modulus of elasticity and the effective density of air, respectively.

By introducing shape functions $[N]^T$, the relationship between p in an element and sound-pressure vector $\{p_e\}$ at the nodal points can be approximated as

$$p = [N]^T \{p_e\} \tag{3}$$

where $[N]^T = [N_1, N_2, N_{3,\ldots}]$ and T denotes the transpose.

Next, the kinetic energy, strain energy, and external work are derived from Eqs. (1)-(3). The following expressions are then obtained by applying the minimum-energy principle.

$$([K]_e - \omega^2 [M]_e)\{p_e\} = -\omega^2 \{u_e\} \tag{4}$$

$$[K]_e = (1/\rho_e)[\tilde{K}]_e \tag{5}$$

$$[M]_e = (1/E_e)[\tilde{M}]_e \tag{6}$$

where ρ_e and E_e are the effective density and bulk modulus of elasticity for gas in an element, respectively, $\{u_e\}$ is the nodal-particle-displacement vector, $[\tilde{M}]_e$ is the matrix containing the shape functions, $[\tilde{K}]_e$ is the matrix containing their derivatives, and $\tilde{M}_{eij}$ and $\tilde{K}_{eij}$ are components of $[\tilde{M}]_e$ and $[\tilde{K}]_e$, respectively. These components can be expressed as follows:

$$\tilde{M}_{eij} = \iiint_e N_i N_j \, dxdydz \tag{7}$$

$$\tilde{K}_{eij} = \iiint_e \{(\partial N_i / \partial x)(\partial N_j / \partial x) + (\partial N_i / \partial y)(\partial N_j / \partial y) + (\partial N_i / \partial z)(\partial N_j / \partial z)\} dxdydz \tag{8}$$

where *i* is the component of the *i*th row, and *j* represents the component of the *j*th column. In this paper, we refer to $[K]_e$ as the stiffness-element matrix and $[M]_e$ as the mass-element matrix.

A model employing complex effective density ρ_e^* and complex propagation speed c_e^* is used to analyze the sonic fields inside sound-absorbing materials [4,5]. In this paper, we use the following model with complex effective density ρ_e^* and complex bulk modulus of elasticity $E_e^* = \rho_e^* (c_e^*)^2$ for the elements in the sound-absorbing materials [4,5]:

$$\rho_e \Rightarrow \rho_e^* = \rho_{eR} + j\rho_{eI} \tag{9}$$

$$E_e \Rightarrow E_e^* = E_{eR} + jE_{eI} \tag{10}$$

Here, j is an imaginary unit and E_{eR} and E_{eI} are the real and imaginary parts of E_e^*, respectively. E_{eI} is related to the hysteresis between sound pressure p and volume strain, $\operatorname{div}\{U\}$. ρ_{eR} and ρ_{eI} are the real and imaginary parts of ρ_e^*, respectively. ρ_{eI} is related to the flow resistance, R. We have verified the effectiveness of this model in our previous study.

The mass-element matrix $[K]_e$ is obtained by substituting Eq. (9) into Eq. (5),

$$[K]_e = [K_R]_e (1 + j\eta_e) \tag{11}$$

where

$$[K_R]_e = (\rho_{eR} / (\rho_{eR}^2 + \rho_{eI}^2))[\tilde{K}]_e, \quad \eta_e = -\rho_{eI} / \rho_{eR} \tag{12}$$

$[K_R]_e$ is the real part of the stiffness-element matrix $[K]_e$. The imaginary part, ρ_{eI}, of the

effective density is related to the flow resistances of sound-absorbing materials, Hence $\eta_e = -\rho_{eI} / \rho_{eR}$ corresponds to material damping due to flow resistance.

By substituting Eq. (10) into Eq. (6), the stiffness-element matrix $[M]_e$ is obtained,

$$[M]_e = [M_R]_e(1 + j\chi_e) \tag{13}$$

where

$$[M_R]_e = (E_{eR} / (E_{eR}^2 + E_{eI}^2))[\tilde{M}]_e, \chi_e = -E_{eI} / E_{eR} \tag{14}$$

$[M_R]_e$ is the real part of $[M]_e$; χ_e is the damping effect due to hysteresis between pressure and volume strain in sound-absorbing materials. All elements of the mixed sonic field can be superposed using Eqs. (4)-(14). This results in the following discrete equation for a global system,

$$\sum_{e=1}^{e_{\max}} \left([K_R]_e(1 + j\eta_e) - \omega^2 [M_R]_e(1 + j\chi_e) \right) \{p_e\} = -\omega^2 \{u\} \tag{15}$$

The sizes of the matrices and vectors in Eq. (15) are modified to be concurrent with the degree of freedom of the global system. $\{u\}$ is the nodal-particle-displacement vector. Both the stiffness and mass matrices for the fields contained in gas and sound-absorbing materials have complex parameters. Eq. (15) describes simultaneous equations with complex parameters. If known values are assigned to the excitation angular frequency ω and the nodal-particle-displacement vector $\{u\}$, Eq. (15) can be solved to obtain an unknown p for the frequency response.

2.2 Calculation of the Contribution of Each Element to Modal Damping

We now present a calculation method to obtain the contributions of each element to modal damping for the mixed sonic fields contained in gas and sound-absorbing materials.

Considering conditions of resonance, the homogeneous equation Eq. (15) corresponds to the following complex-eigenvalue problem:

$$\sum_{e=1}^{e_{\max}} \left([K_R]_e(1 + j\eta_e) - (\omega^{(n)})^2 (1 + j\eta_{tot}^{(n)}) [M_R]_e(1 + j\chi_e) \right) \{\phi^{(n)^*}\} = \{0\} \tag{16}$$

where $e_{\max}$ denotes the number of the elements, $\{\phi^{(n)^*}\}$ is the complex eigenvector, and $\eta_{tot}^{(n)}$ is the modal-loss factor. The superscript (n) denotes the *n*th eigenmode, $(\omega^{(n)})^2$ is the real part of the *n*th complex eigenvalue, and $\omega^{(n)}$ is the *n*th angular-resonant frequency.

Next, the parameters β_{se} and β_{ke} are introduced as

$$\beta_{ke} = \eta_e / \eta_{\max}, \ \beta_{ke} \le 1, \ \beta_{se} = \chi_e / \eta_{\max}, \ \beta_{se} \le 1 \tag{17}$$

where $\eta_{\max}$ is the maximum value among the elements' material-loss factors η_e and χ_e (e = 1, 2, 3, … $e_{\max}$). Under the assumption that $\eta_{\max} << 1$, solutions of Eq. (16) are expanded using the small parameter $\mu = j\eta_{\max}$ as

$$\{\phi^{(n)^*}\} = \{\phi^{(n)}\}_0 + \mu\{\phi^{(n)}\}_1 + \mu^2\{\phi^{(n)}\}_2 + ,... \tag{18}$$

$$(\omega^{(n)})^2 = (\omega_0^{(n)})^2 + \mu^2(\omega_2^{(n)})^2 + \mu^4(\omega_4^{(n)})^2 + ,... \tag{19}$$

$$j\eta_{tot}^{(n)} = \mu\eta_1^{(n)} + \mu^3\eta_3^{(n)} + \mu^5\eta_5^{(n)} + ,... \tag{20}$$

In these equations, under conditions $\beta_{ke} \le 1$, $\beta_{se} \le 1$, and $\eta_{\max} << 1$, we can obtain $\eta_{\max}\beta_{ke} << 1$ and $\eta_{\max}\beta_{se} << 1$. Thus, both $\mu\beta_{se}$ and $\mu\beta_{ke}$ are considered to be small parameters like μ. In these equations, $\{\phi^{(n)}\}_0, \{\phi^{(n)}\}_1, \{\phi^{(n)}\}_2, ...$, $(\omega_0^{(n)})^2$, $(\omega_2^{(n)})^2$, $(\omega_4^{(n)})^2$, ..., and $\eta_1^{(n)}$,

$\eta_3^{(n)}, \eta_5^{(n)}$,... have real quantities.
The following equations are derived by substituting Eqs. (18), (19), and (20) into Eq. (16), and adopting the approximation from the μ^0 order to the μ^1 order:

$$\eta_{tot}^{(n)} = \eta_{ke}^{(n)} - \eta_{se}^{(n)} \tag{21}$$

$$\eta_{ke}^{(n)} = \sum_{e=1}^{e_{\max}} (\eta_e S_{ke}^{(n)}), \eta_{se}^{(n)} = \sum_{e=1}^{e_{\max}} (\chi_e S_{se}^{(n)}),$$

$$S_{ke}^{(n)} = \frac{\{\phi^{(n)}\}^{\mathrm{T}}[K_R]_e\{\phi^{(n)}\}}{\sum_{e=1}^{e_{\max}} \{\phi^{(n)}\}^{\mathrm{T}}[K_R]_e\{\phi^{(n)}\}}, \quad S_{se}^{(n)} = \frac{\{\phi^{(n)}\}^{\mathrm{T}}[M_R]_e\{\phi^{(n)}\}}{\sum_{e=1}^{e_{\max}} \{\phi^{(n)}\}^{\mathrm{T}}[M_R]_e\{\phi^{(n)}\}}$$

From these equations, the modal-loss factor $\eta_{tot}^{(n)}$ can be obtained using the material-loss factors η_e of each element *e* comprising ρ_e^*, each element's share $S_{ke}^{(n)}$ of the total kinetic energy, the material-loss factors, χ_e, of each element *e* comprising E_e^*, and each element's share, $S_{se}^{(n)}$, of the total strain energy. Eigenmodes $\{\phi^{(n)}\}_0$ in Eq. (21) are real, and can be obtained by solving the real eigenvalue problem corresponding to the equation by eliminating all damping terms in Eq. (16).

3. Experimental and Calculation Results

3.1 Experimental setup of test piece

The test piece emulating the upper back, cabin, and trunk of a car is shown in Fig. 1. This enclosed shape is made using acrylic boards with thickness 10 mm, and it enabled it to divide the middle. In case it divides, as for the thickness of the used acrylics board, the bottom fixes an acrylics board as 20 mm, and the acrylics board was made to carry out movable (of the top) up and down (in Fig. 1 red portion). The automobile trim (urethane foam and felt, which are widely used for sound isolation in cars), which is permeable in the gray portion of Fig. 1, was pinched by the up-and-down acrylic boards and considered as two closed spaces differing in magnitude. The key features of this test piece are that urethane foam divides the two closed spaces, and that the magnitude (i.e., area ratio of ventilation material to resin material) of the felt is changeable. In an actual car, the sound property (i.e., balance between sound absorption and sound insulation) will differ for each combination of ventilation and interior materials. Since the ventilation-material ratio is determined by the design, attachment of other parts, intensity, and so forth, the sound property of the optimal ventilation material for each area ratio could be examined for an assumed tire noise. Acoustic input are carried through a pipe to the smaller enclosed space. Mic C was installed near the entrance of the pipe, with Mic B installed near the center of the upper surface. Mic A was placed in between the upper surfaces of the larger and smaller closed spaces. The noise reduction was then calculated.

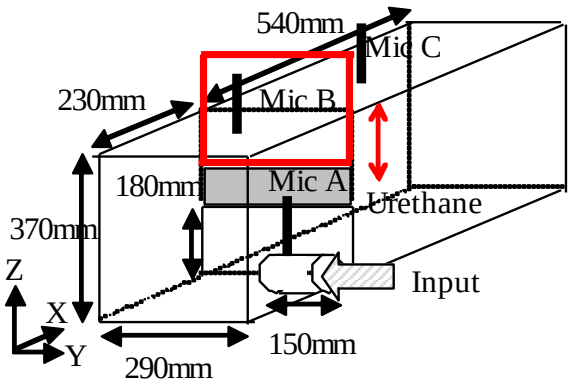

Fig.1 Experimental setup of test piece

3.2 Comparison of Experimental and Calculation Results

The FE model is shown Fig. 2. Altair Hypermesh was used for model creation. The red portion denotes the enclosed spaces, the blue portion represents felt, and the green portion represents urethane foam. Both the urethane foam and felt used here are arranged in a 10 mm thick pile, and the smaller closed space faces the urethane foam while the larger closed space faces felt (refer to Fig. 1). Fig. 3 presents a diagrammatic chart, Fig.3a compares the experimental results and the calculation results of Mic A-B, Fig 3b compares the experimental results and the calculation results of Mic A-C. Mic A-B is noise reduction:

$$\Delta P = 20\log\left|P_B / P_A\right| \quad [\mathrm{dB}] \tag{22}$$

Although some of the peaks have shifted, the microphones mostly reproduce the same result.

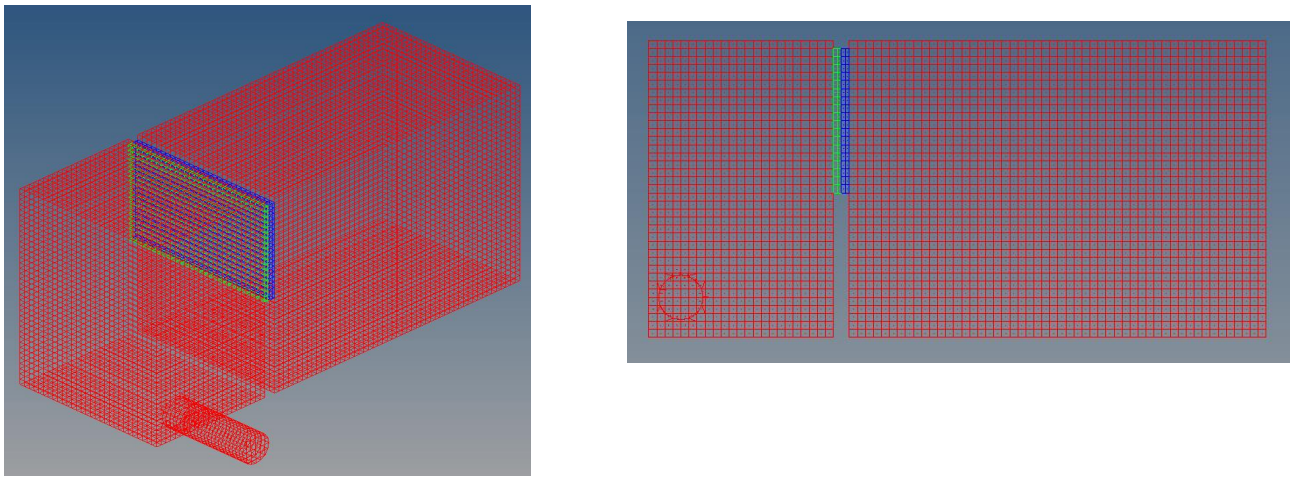

Fig.2 FE model (Air and Urethane foam and Felt)

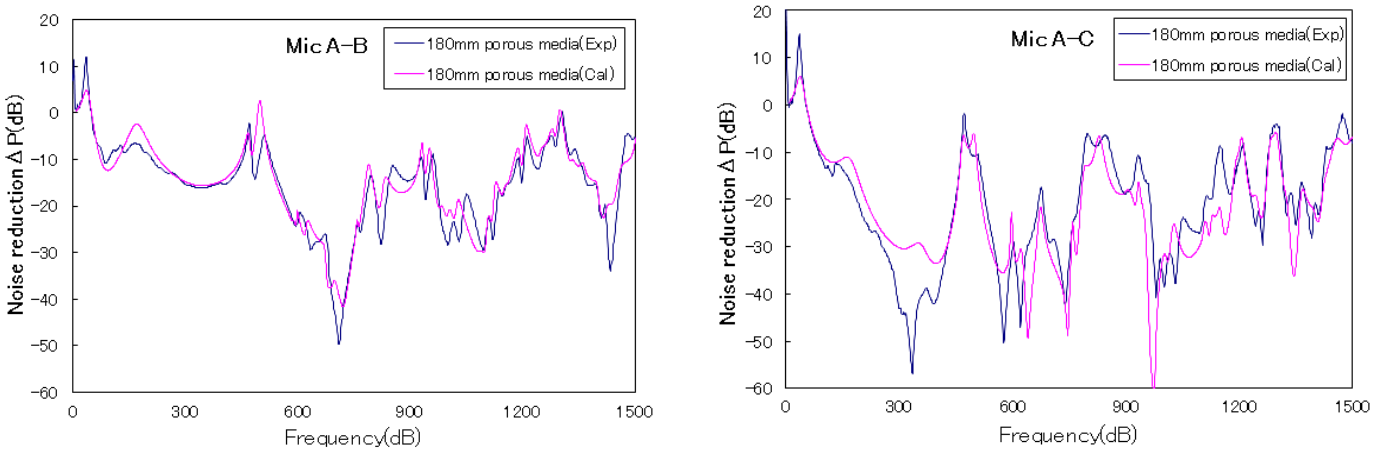

a. noise reduction of Mic A-B b. noise reduction of Mic A-C

Fig.3 Comparison between experimental results and calculation results (porous media)

Next, the thicknesses of urethane foam and felt were varied. The conditions included urethane foam: 0 mm, felt: 20 mm; urethane foam: 5 mm; felt: 15 mm, urethane foam: 15 mm; felt: 5 mm, and urethane foam: 20 mm; felt 0 mm. Noise reduction of Mic A-B and Mic A-C from the 500 Hz band to the 1600 Hz band are shown in Table 1. U in Table 1 is urethane foam and F is felt. Combinations expressed in yellow in Table 1 showed the poorest sound insulation, whereas those in blue show the

best. At Mic A-B, noise in the 1000 Hz and 1250 Hz bands is reduced the most by setting urethane foam thickness to 20 mm. Below the 630 Hz band, noise is reduced by setting felt thickness to 20 mm. At Mic A-C, urethane foam should be thickened for noise reduction, except at 1250 Hz band. A felt thickness of 15 mm leads to greatest noise reduction only at in the 1250 Hz band. Noise-reduction behavior nearly reversed at 1000 Hz for Mc A-B and at 800 Hz for Mic A-C.

Table 1. Calculation results under varied thicknesses of the porous media

Mic A-B	500Hz band	630Hz band	800Hz band	1000Hz band	1250Hz band	1600Hz band
U0 mmF20 mm	−8.70	−27.74	−21.74	−18.98	−9.83	−13.75
U5 mmF15 mm	−8.55	−27.05	−21.62	−19.77	−9.86	−13.77
U10 mmF10 mm	−8.47	−27.11	−21.62	−20.09	−10.19	−14.55
U15 mmF5 mm	−8.37	−26.44	−21.56	−20.96	−10.90	−16.24
U20 mmF0 mm	−8.24	−26.82	−21.84	−21.05	−11.86	−18.52

Mic A-C	500Hz band	630Hz band	800Hz band	1000Hz band	1250Hz band	1600Hz band
U0 mmF20 mm	−16.16	−31.82	−21.24	−28.22	−20.72	−19.54
U5 mmF15 mm	−16.80	−32.06	−21.65	−29.78	−19.99	−19.46
U10 mmF10 mm	−17.22	−32.22	−21.56	−29.66	−19.99	−20.23
U15 mmF5 mm	−17.68	−32.45	−21.79	−29.53	−19.51	−20.12
U20 mmF0 mm	−17.92	−32.54	−21.70	−29.07	−20.13	−21.37

4. Conclusion

A test piece imitating the upper back of a car was created, and the sound absorption between the sound-source side and the car interior due to the arrangement of the trim (urethane foam and felt) was checked by experimental measurement. An FE model was created and the sound-damping characteristics were calculated. Urethane foam and the felt were used to model internal air with a complex effective density and a complex bulk modulus of elasticity. We computed the distributions of the mode-damping contributions of each element in the considered space. This calculation was verified to have sufficient accuracy.

Moreover, we repeated the calculations under various thicknesses of the urethane foam and felt, and determined the combination of thicknesses necessary to reduce maximum noise by a third of an octave. We expect that these results should prove useful in automobile development.

References

[1] M.A. Biot, "Theory of propagation of elastic waves in a fluid-saturated porous solid", ***J. Acoust. Soc. Am.***, Vol. 28, No. 2, pp.168-178, 1955.
[2] J.F. Allard, "Propagation of sound in porous media" in ***Elsevier Applied Science***, 1993.
[3] H. Utsuno, T. Tanaka, and T. Fujikawa, "Transfer function method for measuring characteristic impedance and propagation constant of porous materials", ***J. Acoust. Soc. Am.***, Vol. 86, No. 2, pp.637-643, 1989.
[4] T. Yamaguchi, J. Tsugawa, H. Enomoto, and Y. Kurosawa, "Layout of sound absorbing materials in 3D rooms using damping contributions with eigenvectors as weight coefficients", ***Trans. Jp. Soc. Mech. Eng.***, Vol. 74, No. 747, pp.2648-2654, 2008.
[5] Y. Kurosawa, T. Yamaguchi, and S. Matsumura, "Damped vibration response analysis for automotive panels laminated with damping materials and porous medias", ***Trans. Jp. Soc. Mech. Eng.***, Vol. 77, No. 776C, pp.1191-1200, 2011.

[6] Y. Kurosawa, T. Yamaguchi, "Damped acoustic analysis of an automotive cabin with several porous materials", ***JTSS*** (accepted), 2017.